Heliyon 7 (2021) e06143

Contents lists available at ScienceDirect

Heliyon

journal homepage: www.cell.com/heliyon

Research article

Entropy generation in nanofluid flow due to double diffusive MHD mixed convection

Priyajit Mondal, T.R. Mahapatra *, Rujda Parveen

Department of Mathematics, Visva-Bharati (A Central University), Santiniketan - 731 235, West-Bengal, India

ARTICLE INFO

Keywords:
Entropy generation
MHD mixed convection
Lid driven trapezoidal enclosure
Low aspect ratio
Double diffusive nanofluid flow

ABSTRACT

This work is concerned with the numerical study of laminar, steady MHD mixed convection flow, and entropy generation analysis of Al_2O_3-water nanofluid flowing in a lid-driven trapezoidal enclosure. The aspect ratio of the cavity is taken very small. The cavity is differentially heated to study the fluid flow, heat, and mass transfer rate. The adiabatic upper wall of the enclosure is allowed to move with a constant velocity along the positive x-direction. The second-order finite difference approximation is employed to discretize the governing partial differential equations, and a stream-function velocity formulation is used to solve the coupled non-linear partial differential equations numerically. The simulated results are plotted graphically through streamlines, isotherms, entropy generation, Nusselt number, and Sherwood number. The computations indicate that the average Nusselt number and average Sherwood number are decreasing functions of Hartmann number, aspect ratio, and nanoparticle volume fraction. Significant changes in streamlines, temperature and concentration contours for high Richardson number are observed.

1. Introduction

Minimization of entropy generation is an emerging thermodynamic approach in the field of engineering, which is a major concern to design modern thermal management systems. The concept of entropy generation was first introduced by Bejan (see, [1]). He concluded that the entropy generation minimization process enhances the thermodynamic efficiency of the system and leads to an increment of efficiency of a thermal system. Basak et al. [2] studied the entropy generation for natural convection in a porous cavity considering different boundary conditions of a trapezoidal enclosure with various inclination angles. They analyzed the effects of different Rayleigh number and Prandtl number on the heat transfer rate and entropy generation and found that the magnitude of entropy generation increases with increase in Prandtl number.

Nanofluid is a fluid with suspended metallic nanoparticles of size smaller than 100 nm (see, [3]). The applications of nanofluids on heat transfer have been studied by Buongiorno [4], Das et al. [5], Wen et al. [6], Mahian et al. [7] etc. It is experimentally and theoretically proved that the thermal conductivity of fluid enhanced by 10 - 50 per cent when considering a mixture of a solid volume fraction of nanoparticles less than 5 per cent. Nayak et al. [8] investigated the study of convective heat transfer of a Cu-water nanofluid in a differentially heated skewed enclosure in which nanoparticles are moving at a higher velocity relative to the velocity of the fluid. The result shows that an increment in the nanoparticle size strongly affects the heat transfer rate and the square cavity has maximum heat transfer as compared to all other shapes of the parallelogram enclosure.

Fluids in association with heat and mass transfer are extensively used in substance production, air cooling, refrigeration, transportation, heat exchanger and several other applications (see, [9], [10], [11]). Mixed convection in cavity flow is an important phenomenon due to its various applications in cooling of electronic components, heat exchangers, chemical reactors, solar collectors, food processing, float glass production, thermal-hydraulics of nuclear reactors, flow and heat transfer in solar ponds, dynamics of lakes (see, [12], [13], [14], [15]) etc. Keeping this motivation in mind in many engineering applications forced convection is encountered in the analysis of pipe flow, cavity flow, flow over a flat plate, heat exchangers etc. Mixed convection and entropy generation of Cu-water nanofluid and pure water in a lid-driven square cavity have been studied by Khorasanizadeh et al. [16]. They reported that for a suitable choice of Reynolds number and Rayleigh number, heat transfer enhancement and minimum entropy generation are obtained. Nayak et al. [17] examined the entropy generation and mixed convection of Cu-water nanofluid inside a differentially heated skew enclosure and studied the heat transfer, fluid flow and entropy generation

* Corresponding author.
E-mail address: trmahapatra@yahoo.com (T.R. Mahapatra).

https://doi.org/10.1016/j.heliyon.2021.e06143
Received 22 April 2020; Received in revised form 24 June 2020; Accepted 27 January 2021

Table 1. Thermophysical properties of water and Aluminium oxide nanoparticle [26].

Properties	water	Al_2O_3 nanoparticles
$C_p(J\ kg^{-1}\ K^{-1})$	4179	765
$k(W\ m^{-1}\ K^{-1})$	0.623	40
$\rho(kg\ m^{-3})$	997.1	3970
$\beta_T(K^{-1})$	21×10^{-5}	0.8×10^{-5}
$\sigma(kg^{-1}\ m^{-3}\ s^3\ A^2)$	0.05	3.69×10^{7}
$\mu(kg\ m^{-1}\ s^{-1})$	0.001003	-
$\alpha(m^2\ s^{-1})$	0.143×10^{-6}	-

due to the addition of nanoparticles and different skew angle. They observed that heat transfer enhancement is achieved for a higher value of the skew angle. Magnetic field plays an important role in the fluid flow due to the presence of Lorentz force that highly effects the heat and mass transfer rate. Elshehabey and Ahmed [18] studied the mixed convection flow in the presence of a magnetic field using Buongiorno's nanofluid model with sinusoidal temperature distribution. They found that the fluid movement retards due to the presence of an inclined magnetic field.

Various studies are performed on different geometries, such as: A numerical modelling of steady laminar mixed convection flow of water-Al_2O_3 nanofluid in a lid-driven inclined square enclosure has been discussed by Abu-Nada and Chamkha [19], Waheed [20] has studied heat transfer of mixed convection flow in rectangular enclosures with moving horizontal plate, mixed convection flow in a trapezoidal enclosure filled with two layers of nanofluid and porous media with a rotating circular cylinder and a sinusoidal bottom wall was studied by Hussein et al. [21], numerical investigation of double diffusive natural convection and entropy generation of nanofluid in a wavy enclosure with discrete heating in the presence of magnetic field have been discussed by Parveen and Mahapatra [22], Chamkha et al. [23] recently studied effects of a rotating cone on the mixed convection in a double lid-driven 3D porous trapezoidal cavity filled with nanofluid under the impact of magnetic field, mixed convection of hybrid nanofluid in a porous trapezoidal chamber was discussed by Cimpean et al. [24] etc. In the analysis of entropy generation, the geometry of the cavity is also considerable as it varies for different shape of cavities. In the present study, a trapezoidal enclosure with various aspect ratios is considered.

In this manuscript, double-diffusive mixed and forced convection of nanofluid inside a trapezoidal cavity of low aspect ratio ($0.2 \le A \le 0.4$) with moving upper wall in the presence of magnetic field acting perpendicularly to the $x-$axis has been analyzed. Previously, entropy generation has been studied in many researches, but all the reasons (viz. fluid flow, heat transfer, mass transfer and magnetic field) of entropy generation have not been analyzed together in a low aspect ratio trapezoidal enclosure for double-diffusive MHD mixed convection flow. In the present manuscript, those limitations are overcome with a lot of effects, which are basically observed in most of the real applications and therefore, the present study can be used as a more general entropy generation minimization process. The main objective of the present study is to investigate and minimize the entropy generation due to the combined effects of heat and mass transfer, fluid flow and magnetic field in a low aspect ratio cavity, which may be applied to improve several thermodynamic applications like refrigeration, cooling of electronic equipment, heat exchangers by increasing their efficiency as well as making them thinner.

2. Problem formulation

2.1. Thermo-physical properties of nanofluid

According to the Boussinesq model thermo-physical properties of the nanofluid are assumed to be constant except for the variation of density. Thermo-physical properties of water and Al_2O_3 nanoparticles are given in Table 1.

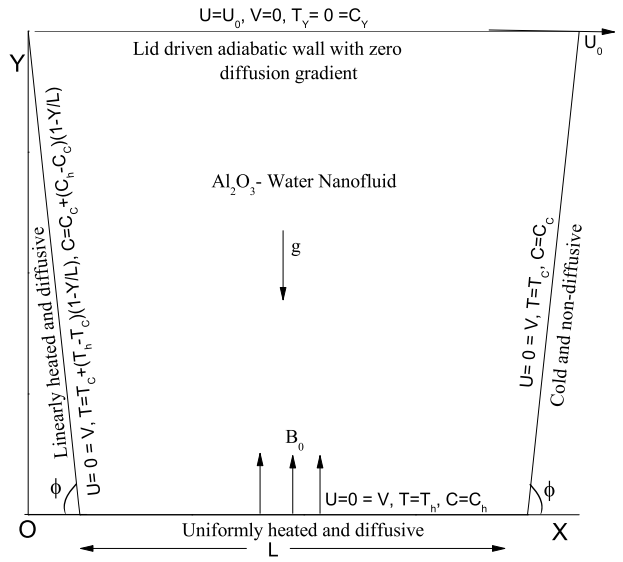

Physical model of the problem

Fig. 1. Physical diagram of the considered problem.

The thermal diffusivity, effective density, heat capacitance of nanofluid, thermal expansion coefficient and solutal expansion coefficient are given by Xuan and Roetzel [25] as

$$\alpha_{nf}=\frac{k_{nf}}{(\rho c_p)_{nf}},\ \rho_{nf}=(1-\varphi)\rho_f+\varphi\rho_s,\ (\rho c_p)_{nf}=(1-\varphi)(\rho c_p)_f+\varphi(\rho c_p)_s,$$

$$(\rho\beta_T)_{nf}=(1-\varphi)(\rho\beta_T)_f+\varphi(\rho\beta_T)_s \text{ and } (\rho\beta_S)_{nf}=(1-\varphi)(\rho\beta_S)_f+\varphi(\rho\beta_S)_s,$$

respectively. The effective thermal conductivity (k_{nf}) and viscosity (μ_{nf}) of nanofluid followed respectively by Maxwell-Garnetts model [27] and Brinkman relation [28] and are given by

$$k_{nf}=k_f\left[\frac{k_s+2k_f-2\varphi(k_f-k_s)}{k_s+2k_f+\varphi(k_f-k_s)}\right] \text{ and } \mu_{nf}=\frac{\mu_f}{(1-\varphi)^{2.5}},$$

where k, ρ, φ, β_T, β_S, C_p are thermal conductivity, fluid density, nanoparticle volume fraction, coefficient of thermal expansion, coefficient of solutal expansion respectively and the suffixes s, f, nf refer to the corresponding properties nanoparticles, base fluid, nanofluid, respectively.

2.2. Governing equations and boundary conditions

The two-dimensional governing equations for viscous, steady, magnetohydrodynamic, double-diffusive, mixed convection flow of water-based Al_2O_3 nanofluid inside a trapezoidal cavity with right and left walls inclined at an angle ϕ with the positive X-axis and the negative X-axis, respectively are based on the law of conservation of mass, linear momentum, thermal energy and concentration. In the present study, the cavity is considered with uniformly heated and diffusive bottom wall, adiabatic and of zero concentration gradient top wall, linearly heated and diffusive left wall, cold and non-diffusive right wall. The top wall of the cavity is moving with velocity U_0 in the positive X-direction. A uniform magnetic field B_0 is imposed along Y-axis neglecting the induced magnetic field, which is justified for MHD flow at small magnetic Reynolds number [29]. The physical model of the problem is shown in Fig. 1.

Mass flux due to temperature gradient is known as Soret effect and its impact on the liquid is important only when the concentration of solute is not small but in the present study, the concentration of solute in the liquid is small. So the Soret effect is neglected. The reciprocal phenomenon to the Soret effect is Dufour effect, which is the energy flux

due to the concentration of solute occurring as a coupled effect of irreversible processes. It is also negligible as the energy flux due to mass concentration in the liquid is very small. Chemical reactions are also neglected because Al_2O_3 is a stable compound as in the structure of Al_2O_3 there are four aluminium atoms around the oxygen atom as tetrahedral and six oxygen atoms around the aluminium atom as octahedral, which mean both atoms have the maximum coordination number according to valence bond theory. So that there is no possibility to get a reaction between aluminium oxide and water.

The thermo-physical properties are treated as constant except in the buoyancy term where the density, is considered as a function of temperature and concentration under Boussinesq approximation. The equations of continuity, momentum, energy and concentration for the problem under consideration can be written in dimensional form as follows:

$$U_X + V_Y = 0, \tag{1}$$

$$UU_X + VU_Y = -\frac{1}{\rho_{nf}} P_X + \nu_{nf}(U_{XX} + U_{YY}) - \frac{\sigma_{nf} B_0^2 U}{\rho_{nf}}, \tag{2}$$

$$UV_X + VV_Y = -\frac{1}{\rho_{nf}} P_Y + \nu_{nf}(V_{XX} + V_{YY}) + \frac{g(\rho\beta_T)_{nf}}{\rho_{nf}}(T - T_c) + \frac{g(\rho\beta_S)_{nf}}{\rho_{nf}}(C - C_c), \tag{3}$$

$$UT_X + VT_Y = \alpha_{nf}(T_{XX} + T_{YY}), \tag{4}$$

$$UC_X + VC_Y = D(C_{XX} + C_{YY}), \tag{5}$$

where U, V, P, T, C, D, g, T_C, C_C, σ_{nf}, ν_{nf} represent dimensional velocity along X-direction, dimensional velocity along Y-direction, dimensional pressure, dimensional temperature, dimensional concentration, mass diffusivity, acceleration due to gravity, dimensional temperature at the cold wall, dimensional concentration at the non-diffusive wall, electrical conductivity of nanofluid, kinematic viscosity of nanofluid respectively and the suffixes X, Y represent the partial derivative with respect to X, Y respectively.

The imposed dimensional boundary conditions for considered problem are as follows:

(i) at the top wall: $U = U_0, V = 0, T_Y = 0 = C_Y$,
(ii) at the bottom wall: $U = V = 0, T = T_h, C = C_h$,
(iii) at the left wall: $U = V = 0, T = T_c + (T_h - T_c)(1 - Y/L), C = C_c + (C_h - Cc)(1 - Y/L)$,
(iv) at the right wall: $U = V = 0, T = T_c, C = C_c$.

Introducing the non-dimensional variables $x = X/L, y = Y/L, u = U/U_0, v = V/U_0, p = P/(\rho_{nf} U_0^2), \theta = (T - T_c)/(T_h - T_c), S = (C - C_c)/(C_h - C_c)$, the governing Eqs. (1) - (5) can be written in the dimensionless form as:

$$u_x + v_y = 0, \tag{6}$$

$$uu_x + vu_y = -p_x + \frac{\mu_{nf}}{\rho_{nf}\nu_f}\frac{1}{Re}(u_{xx} + u_{yy}) - \frac{\sigma_{nf}\rho_f}{\sigma_f\rho_{nf}}\frac{Ha^2}{Re}u, \tag{7}$$

$$uv_x + vv_y = -p_y + \frac{\mu_{nf}}{\rho_{nf}\nu_f}\frac{1}{Re}(v_{xx} + v_{yy}) + \frac{(\rho\beta_T)_{nf}}{\rho_{nf}\beta_f} Ri(\theta + NS), \tag{8}$$

$$u\theta_x + v\theta_y = \frac{\alpha_{nf}}{\alpha_f}\frac{1}{RePr}(\theta_{xx} + \theta_{yy}), \tag{9}$$

$$uS_x + vS_y = \frac{1}{LePrRe}(S_{xx} + S_{yy}), \tag{10}$$

where $Pr\left(=\frac{\nu_f}{\alpha_f}\right)$, $Re\left(=\frac{U_0 L}{\nu_f}\right)$, $Le\left(=\frac{\alpha_f}{D}\right)$, $Ha\left(=\sqrt{\frac{\sigma_f}{\mu_f}}B_0 L\right)$, $Gr\left(=\frac{g\beta_f(T_h - T_c)L^3}{\nu_f^2}\right)$, $Ri\left(=\frac{Gr}{Re^2}\right)$, $N\left(=\frac{(\rho\beta_S)_{nf}(C_h - C_c)}{(\rho\beta_T)_{nf}(T_h - T_c)}\right)$, u, v, p, θ, S are the Prandtl number, Reynolds number, Lewis number, Hartmann number, Grashof number, Richardson number, Buoyancy ratio, dimensionless velocity along x-axis, dimensionless velocity along y-axis, dimensionless pressure, dimensionless temperature, dimensionless concentration respectively and the suffixes x, y represent the partial derivative with respect to x, y respectively and the dimensionless boundary conditions become:

(i) at the top wall: $u = 1, v = 0, \theta_y = 0 = S_y$,
(ii) at the bottom wall: $u = v = 0, \theta = 1 = S$,
(iii) at the left wall: $u = v = 0, \theta = 1 - y = S$,
(iv) at the right wall: $u = v = 0, \theta = 0 = S$.

The non-dimensional streamfunction (ψ) and vorticityfunction (ω) are defined by the equations:

$$u = \psi_y, v = -\psi_x \text{ and } \omega = v_x - u_y, \tag{11}$$

which yields a single equation as:

$$\psi_{xx} + \psi_{yy} = -\omega. \tag{12}$$

Eliminating p from (7) and (8) and using Eqs. (11), one can find

$$\frac{1}{Re}\left(\frac{\mu_{nf}}{\rho_{nf}\nu_f}\right)(\omega_{xx} + \omega_{yy}) - (u\omega_x + v\omega_y) + \frac{(\rho\beta_T)_{nf}}{\rho_{nf}\beta_{nf}} Ri(\theta_x + NS_x) + \frac{\sigma_{nf}\rho_f}{\sigma_f\rho_{nf}}\frac{Ha^2}{Re}u_y = 0. \tag{13}$$

2.3. Nusselt number

The rate of heat transfer at the boundaries in terms of Nusselt number (Nu) is the ratio of convective heat transfer to conductive heat transfer and is defined as: $\mathrm{Nu} = \frac{q_c}{k_f(T_h - T_c)/L} = \frac{Lq_c}{k_f(T_h - T_c)}$, $q_c = -k_{nf}\left(\frac{\partial T}{\partial n^*}\right)_{n^*=0}$, where q_c is the surface heat flux and n^* is the dimensional direction in the outward drawn normal. Using the non-dimensional variables $\theta = (T - T_c)/(T_h - T_c), n = n^*/L$, Nusselt number can be written as: $\mathrm{Nu} = -\left(\frac{k_{nf}}{k_f}\right)\theta_n$, where n is the non-dimensional normal direction to the plane and θ_n is the partial derivative of θ with respect to n. The local Nusselt number at the top, bottom, left and right walls are respectively given by:

$$\mathrm{Nu}_t = -\left(\frac{k_{nf}}{k_f}\right)\theta_y|_{y=A},\ \mathrm{Nu}_b = \left(\frac{k_{nf}}{k_f}\right)\theta_y|_{y=0},$$
$$\mathrm{Nu}_l = \left(\frac{k_{nf}}{k_f}\right)\left[\theta_x|_l \sin\phi + \theta_y|_l \cos\phi\right],$$
$$\mathrm{Nu}_r = -\left(\frac{k_{nf}}{k_f}\right)\left[\theta_x|_r \sin\phi - \theta_y|_r \cos\phi\right], \tag{14}$$

and average Nusselt numbers at the bottom, left and right walls are defined as:

$$\overline{\mathrm{Nu}_b} = \int_0^1 \mathrm{Nu}_b\, dx,\ \overline{\mathrm{Nu}_l} = \frac{\sin\phi}{A}\int_0^{\frac{A}{\sin\phi}} \mathrm{Nu}_l\, dS_1,\ \overline{\mathrm{Nu}_r} = \frac{\sin\phi}{A}\int_0^{\frac{A}{\sin\phi}} \mathrm{Nu}_r\, dS_2$$

respectively and the overall average Nusselt number

$$\overline{\mathrm{Nu}} = (\overline{\mathrm{Nu}_b} + \overline{\mathrm{Nu}_l} + \overline{\mathrm{Nu}_r})/3, \tag{15}$$

where dS_1 and dS_2 are the small elemental lengths along the left and right walls, respectively. Here, $\mathrm{Nu}_t = 0$ as the top wall of the considered problem is adiabatic.

2.4. Sherwood number

The ratio of convective mass transfer and diffusive mass transfer, known as Sherwood number (Sh) is defined as: $Sh = -S_n$, where n is

the normal direction to the plane. The local Sherwood number at the top, bottom, left and right walls are respectively given by:

$$Sh_t = -S_y|_{y=A},\ Sh_b = S_y|_{y=0}, Sh_l = \left[S_x|_l \sin\phi + S_y|_l \cos\phi\right],$$
$$Sh_r = -\left[S_x|_r \sin\phi - S_y|_r \cos\phi\right], \tag{16}$$

and average Sherwood numbers at the bottom, left and right walls are defined as:

$$\overline{Sh}_b = \int_0^1 Sh_b\, dx,\ \overline{Sh}_l = \frac{\sin\phi}{A}\int_0^{\frac{A}{\sin\phi}} Sh_l\, dS_1, \overline{Sh}_r = \frac{\sin\phi}{A}\int_0^{\frac{A}{\sin\phi}} Sh_r\, dS_2$$

respectively and the overall average Sherwood number

$$\overline{Sh} = (\overline{Sh}_b + \overline{Sh}_l + \overline{Sh}_r)/3, \tag{17}$$

where dS_1 and dS_2 are the small elemental lengths along the left and right walls, respectively. Here, $Sh_t = 0$ as the top wall of the cavity is of zero diffusive gradient.

2.5. Entropy generation

According to the local thermodynamic equilibrium of linear transport theory, the dimensionless local entropy generation due to fluid friction, heat transfer, mass transfer and magnetic field in Cartesian co-ordinate are given by (see, [30] and [31])

$$S_\psi = \lambda_1 \left(\frac{\mu_{nf}}{\mu_f}\right)\left[2\left(u_x^2 + v_y^2\right) + \left(u_y + v_x\right)^2\right], \tag{18}$$

$$S_\theta = \left(\frac{k_{nf}}{k_f}\right)\left[\theta_x^2 + \theta_y^2\right], \tag{19}$$

$$S_\tau = \lambda_2\left[S_x^2 + S_y^2\right] + \lambda_3\left[\theta_x S_x + \theta_y S_y\right], \tag{20}$$

$$S_M = \lambda_1 \left(\frac{\mu_{nf}}{\mu_f}\right) Ha^2 u^2, \tag{21}$$

where λ_1, λ_2 and λ_3 are irreversibility distribution ratios and they are taken as $\lambda_1 = 0.0001, \lambda_2 = 0.5$ and $\lambda_3 = 0.01$ ([22]).

3. Co-ordinate transformation and numerical procedure

Application of boundary conditions at different boundaries of an irregular enclosure is not a simple task. Again, prescriptions of conditions at boundaries not conforming to the co-ordinate lines lead to severe interpolation errors. For these reasons a transformation is introduced to map the irregular physical domain to a square computational domain where we can use a uniform grid. The coordinate transformation used in this study is:

$$\xi = \frac{x + y\cot\phi}{1 + 2\ y\ \cot\phi},\ \eta = \frac{y}{A}. \tag{22}$$

This transformation maps the trapezoidal physical domain (in $x - y$ plane) to a computational square domain (in $\xi - \eta$ plane).

Using the transformation (22), Eqs. (13), (9) and (10) are transformed as:

$$\left(\frac{\mu_{nf}}{\rho_{nf}\nu_f Re}\right)\left[\left(G^2 + \frac{A^2E^2}{4}\right)\omega_{\xi\xi} + E\omega_{\xi\eta} + \frac{1}{A^2}\omega_{\eta\eta}\right]$$
$$+\left[\left(\frac{\mu_{nf}}{\rho_{nf}\nu_f}\right)\frac{H}{Re} - uG - \frac{vAE}{2}\right]\omega_\xi - \frac{v}{A}\omega_\eta + \frac{(\rho\beta_T)_{nf}}{\rho_{nf}\beta_f}Ri\left(G\theta_\xi + NGS_\xi\right)$$
$$+\frac{\sigma_{nf}\rho_f}{\sigma_f\rho_{nf}}\frac{Ha^2}{Re}\left(\frac{AE}{2}u_\xi + \frac{1}{A}u_\eta\right) = 0, \tag{23}$$

$$\left[\left(uG + \frac{vAE}{2}\right) - \frac{\alpha_{nf}}{\alpha_f}\frac{H}{RePr}\right]\theta_\xi + \frac{v}{A}\theta_\eta$$
$$= \frac{\alpha_{nf}}{\alpha_f}\frac{1}{RePr}\left[F\theta_{\xi\xi} + E\theta_{\xi\eta} + \frac{1}{A^2}\theta_{\eta\eta}\right], \tag{24}$$

$$\left[\left(uG + \frac{vAE}{2}\right) - \frac{H}{LeRePr}\right]S_\xi + \frac{v}{A}S_\eta$$
$$= \frac{1}{LeRePr}\left[FS_{\xi\xi} + ES_{\xi\eta} + \frac{1}{A^2}S_{\eta\eta}\right], \tag{25}$$

where G, E, F and H are given by $G = 1/(1 + 2\ A\eta\ cot\phi)$, $E = (2(1 - 2\ \xi)\ cot\phi)/(A(1 + 2A\eta\ cot\phi))$, $F = G^2 + A^2E^2/4$ and $H = -(4(1 - 2\xi)cot^2\phi)/(1 + 2\ A\eta\ cot\phi)^2$.

We have not found any way to solve the Eqs. (23) - (25) analytically because they are coupled non-linear partial differential equations. So the Eqs. (23) - (25) are discretized using second order central difference formula of ψ, θ and S as described by Mahapatra and Mondal [32]. The matrix form of the discretized Eqs. (23) - (25) are:

$$A_1\boldsymbol{\psi} = \boldsymbol{f}(Pr, Re, Ri, Ha, N, A, u, v, \theta, \psi_\xi, \psi_\eta, S), \tag{26}$$

$$A_2\boldsymbol{\theta} = \boldsymbol{0}, \tag{27}$$

$$A_3\boldsymbol{S} = \boldsymbol{0}, \tag{28}$$

where the co-efficient matrices A_1, A_2 and A_3 are of order mn and the number of components in the vectors $\boldsymbol{\psi}$, $\boldsymbol{\theta}$, $\boldsymbol{S}$ and $\boldsymbol{f}$ is mn for a grid size m × n. The governing Eqs. (6) - (10) are non-linear and the use of non-uniform grid leads to non-symmetric matrices which motivates us to use biconjugate gradient stabilized method (BiCGStab) (see, [33]) that constitutes inner iterations. The Eqs. (26) - (28) are solved by outer - inner iteration process discussed by Gupta and Kalita [34]. The convergence is assumed to reach when the absolute errors between two consecutive iterations are less than 0.5×10^{-6}. The iterations are performed for ψ, θ and S. The CPU usage and running time for the applied numerical method are 99 % and 841.37 seconds for a grid size of 81×81 and for the case of $A = 0.3$, $Re = 100$, $Ri = 0.01$, $Le = 1$, $N = 5$, $Ha = 40$ and $\varphi = 0.03$ respectively. At last the entropy generations (S_ψ), (S_θ), (S_τ) and (S_M) are obtained from the discretized forms of Eqs. (18) - (21).

4. Results and discussion

In the present study, streamfunctions, isotherms, isoconcentrations and the minimization of entropy generation due to the combined effects of fluid friction, heat transfer, mass transfer and magnetic field for mixed convection flow of Al_2O_3 nanofluid inside a trapezoidal enclosure with moving upper wall having constant velocity are discussed. The aspect ratio is considered as very low $(0.2 - 0.3)$. There is a magnetic field acting perpendicularly in the positive y direction on the horizontal walls of the cavity. Some parameters are considered fixed, which are Prandtl number $(Pr = 6.2)$, Buoyancy ratio $(N = 1)$, Reynolds number $(Re = 100)$ and the inclination angle of right and left walls of the cavity with the positive and negative x-axis respectively as $\phi = 60^0$. No-slip boundary conditions at the inclined walls and bottom wall of the cavity are implemented. Together with these, linearly heated and diffusive left wall, cold and non-diffusive right wall, uniformly heated and diffusive bottom wall and adiabatic with zero diffusion gradient top wall are considered.

4.1. Validation of the code and grid independence test

To verify the accuracy of the results, a comparison has been performed for the values of $|\psi|_{max}$ and $\overline{Nu}$ with the benchmark numerical solutions discussed by Basak et al. [2]. The present result is compared for the flow of fluid inside a square cavity with hot left wall, cold right wall, adiabatic top and bottom walls for $Pr = 0.71$ and $Ra = 10^3$ and 10^4, $Ha = 0$, which gives a good accuracy of the present result shown in Table 2. Also, a comparison has been performed for $|\psi|_{max}$ and $\overline{Nu}$ for natural convection flow inside a square cavity of water-Al_2O_3 nanofluid in the presence of magnetic field studied by Ghasemi et al. [35] for $Ra = 10^3$, $Ha = 60$ and $\varphi = 0.03$ are shown in Table 3, which shows a good agreement with the present result.

Table 2. Comparison of the results with Basak et al. [2].

	Basak et al. [2]		Present	
Ra	$\lvert\psi\rvert_{max}$	$\overline{Nu}$	$\lvert\psi\rvert_{max}$	$\overline{Nu}$
10^3	1.1746	1.1179	1.1727	1.1183
10^4	5.0737	2.2482	5.0745	2.2446

Table 3. Comparison of the results with Ghasemi et al. [35].

	Ghasemi et al. [35]		Present	
Ra	$\lvert\psi\rvert_{max}$	$\overline{Nu}$	$\lvert\psi\rvert_{max}$	$\overline{Nu}$
10^3	0.110	1.121	0.108	1.117
10^4	1.057	1.249	1.053	1.244
10^5	5.642	3.124	5.639	3.120

Table 4. Grid independence test of $\lvert\psi\rvert_{max}$ for $A = 0.2$, $Re = 100$, $Ri = 1$, $Le = 1$, $N = 1$, $Ha = 20$, $\varphi = 0.05$ and $\phi = 60^0$.

Grid	21×21	41×41	81×81	161×161
$\lvert\psi\rvert_{max}$	2.7131	2.71146	2.6921	2.6916

To check whether the solution obtained depends on the grid used, we have checked the results for different grid sizes. A grid independence study is performed for $\lvert\psi\rvert_{max}$ with the grid sizes 21×21, 41×41, 81×81 and 161×161 and presented in Table 4, which shows that the results are almost same. So we have performed all the computations using 81×81 grid.

4.2. Numerical discussion

Numerical results of streamlines, isotherms, isoconcentrations and entropy generation due to fluid flow, heat transfer, mass transfer, and magnetic field are illustrated in Figs. 2, 3, 4, 5, 6 for different values of the parameters $Ha(20-40), \varphi(0.01-0.1), Le(1-2), Ri(0.01-100)$ and $A(0.2-0.4)$ in a trapezoidal cavity with linearly heated and diffusive left wall, uniformly heated and a diffusive bottom wall, cold and of zero diffusion gradient right wall, the adiabatic top wall having zero diffusion gradient. Here Pr is taken as 6.2 and the inclination angle of the right wall of the cavity with the positive x-axis and that of the left wall of the cavity with the negative x-axis is 60^0.

Figs. 2(a)-2(b) represent the contours of streamlines, isotherms and isoconcentrations for $Ri = 1$, $Ha = 20$, $N = 1$, $Le = 1$, $Re = 100$ and for $A = 0.2$ and 0.3 with $\lvert\psi\rvert_{max} = 0.1334 (A = 0.2)$, $0.1071 (A = 0.3)$. It is observed that aspect ratio is an important parameter for the flow inside the cavity. As aspect ratio decreases the volume of the cavity decreases, which results in an increment in the fluid flow in a low aspect ratio cavity. The flow is circulating towards the right wall of the cavity as the upper wall is moving with a fixed velocity U_0 and it is also observed that as the aspect ratio increases the fluid inside the cavity is flowing in a larger circular path. The isotherm and isoconcentration contours spread from linearly heated and diffusive left wall towards the right-bottom corner as it is the junction of two hot, diffusive and cold, non-diffusive walls of the cavity.

In thermal convection and mass diffusion problems, the Richardson number has an important role to present the forced convection flow relative to mixed convection flow. If $Ri << 1.0$ forced convection dominates the flow and for $Ri = 1.0$ mixed convection phenomenon is observed whereas for $Ri >> 1$ free convection dominates. Figs. 3(a) - 3(d) represent the contours of ψ, θ and S for $Ha = 40, N = 1, Le = 1, Re = 100, A = 0.3, \varphi = 0.05$ and for different values of Ri (0.01 in Fig. 3(a), 0.1 in Fig. 3(b), 1.0 in Fig. 3(c) and 100 in Fig. 3(d)). In Figs. 3(a) and 3(b), the streamlines represent the flow when forced convection dominates over free convection whereas the streamlines in Fig. 3(c) represent the flow when forced convection and free convection are of the same order. Fig. 3(d) shows the streamlines when free convection dominates over forced convection. In this figure, two circulations are seen near the hot left wall and cold right wall. The values of $\lvert\psi\rvert_{max}$ are 1.8992 (for $Ri = 0.01$), 1.9231 (for $Ri = 0.1$), 2.2243 (for $Ri = 1.0$) and 0.3303 (for $Ri = 100$). When $Ri \leq 1$, strength of flow increases as Ri increases but when $Ri \geq 1$, strength of flow decreases as Ri increases. The contours of θ and S in Figs. 3(a) - 3(d) represent heat and mass transfer phenomena inside the cavity. In Figs. 3(a) - 3(c), it is observed that heat and mass transfer phenomena are almost the same due to mixed and forced convection but in Fig. 3(d) different type of contours are found relative to Figs. 3(a) - 3(c) which is caused by free convection.

Figs. 4(a) - 4(c) represent the contours of ψ, θ and S for $Ri = 1$, $Ha = 40$, $N = 1$, $Le = 2$, $Re = 100$, $A = 0.3$ and for $\varphi = 0.01$, 0.05 and 0.1 respectively with $\lvert\psi\rvert_{max} = 2.7376$ (for $\varphi = 0.01$), 2.5861 (for $\varphi = 0.05$) and 2.4384 (for $\varphi = 0.1$). It is observed that the strength of flow is decreasing with the increment of nanoparticles in the Al_2O_3-water nanofluid. Streamlines are circulated from left to right and due to lid-driven upper wall circulations are observed towards the right wall and they are dense near the right wall. A few interesting patterns of the contours of isotherms and isoconcentrations are observed and found to be distorted and compressed at the right bottom corner, which is the junction of hot, diffusive and cold non-diffusive walls for $0.01 \leq \varphi \leq 0.1$.

Comparing Figs. 3(c) and 4(b) it can be seen that heat transfer phenomenon represented by the contours of θ are highly distributed towards the upward direction in Fig. 4(b) than that in Fig. 3(c) but mass transfer phenomenon represented by the contours of S are highly distributed towards the upward direction in Fig. 3(c) than that in Fig. 4(b). These effects are caused by the Lewis number.

Figs. 5(a) - 5(c) represent the contours of pointwise entropy generation caused by the effect of fluid flow, heat transfer, mass transfer and magnetic field and the contours of pointwise total entropy generation for $Ri = 1$, $Ha = 20$, $N = 5$, $Le = 1$, $Re = 100$, $A = 0.3$ and the effect of Al_2O_3 nanoparticles volume fraction (φ) in water is observed. Entropy generations due to fluid friction (S_ψ) and magnetic field (S_M) are much less than that due to heat transfer (S_θ) and mass transfer (S_τ). The maximum absolute values of entropy generations are $\lvert S_\psi\rvert_{max} = 31.65$ (for $\varphi = 0.01$ in Fig. 5(a)), 35.087 (for $\varphi = 0.05$ in Fig. 5(b)) and 40.165 (for $\varphi = 0.1$ in Fig. 5(c)), $\lvert S_\theta\rvert_{max} = 317573$ (for $\varphi = 0.01$ in Fig. 5(a)), 355091 (for $\varphi = 0.05$ in Fig. 5(b)) and 406448 (for $\varphi = 0.1$ in Fig. 5(c)) and $\lvert S_\tau\rvert_{max} = 157407$ (for $\varphi = 0.01$, 0.05 and 0.1). S_ψ contours are congested towards the boundary of the cavity and it is increasing with the increment of φ. The same phenomenon is observed for S_θ and S_τ but they are congested in the right bottom corner, which is the junction of hot and cold walls. $\lvert S_M\rvert_{max}$ is also increasing with

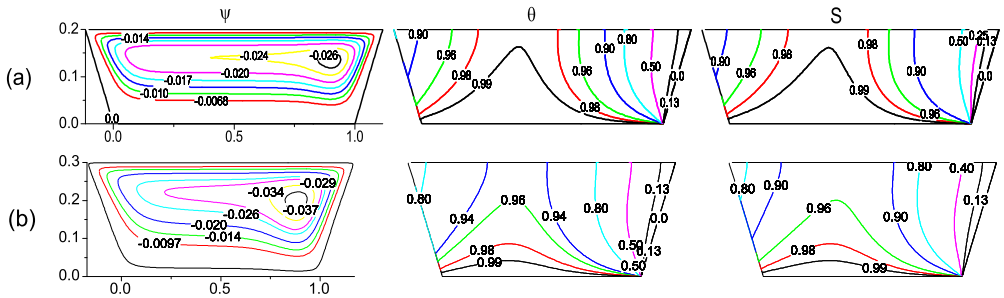

Fig. 2. Streamlines (ψ), isotherms (θ) and isoconcentrations (S) for $Ri = 1$, $Ha = 20$, $N = 1$, $Le = 1$, $Re = 100$ and $\varphi = 0.05$ for (a) $A = 0.2$ and (b) $A = 0.3$.

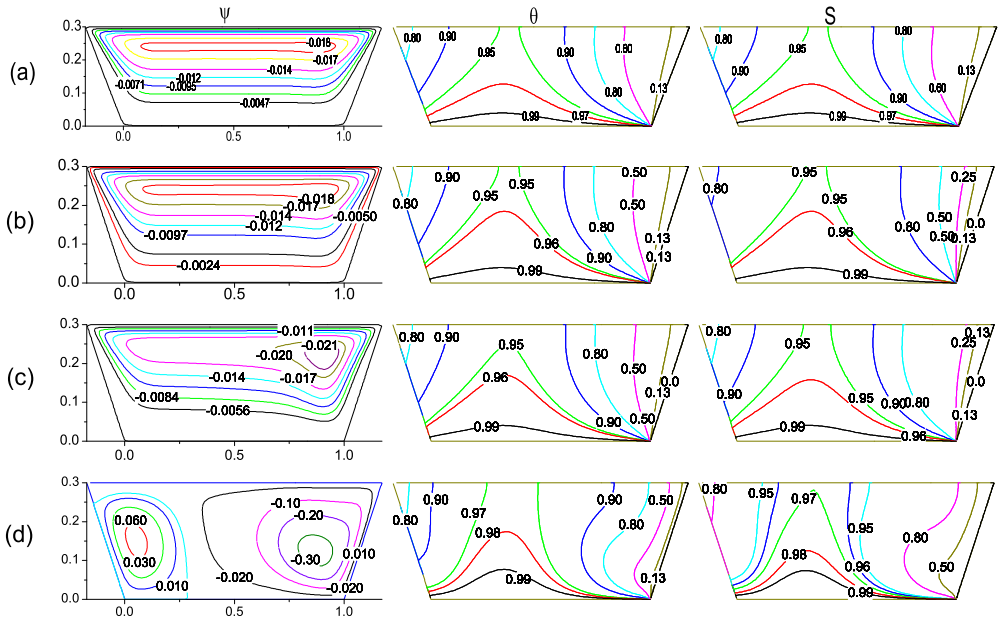

Fig. 3. Streamlines (ψ), isotherms (θ) and isoconcentrations (S) for $Ha = 40$, $N = 1$, $Le = 1$, $Re = 100$, $A = 0.3$ and $\varphi = 0.05$ for (a) $Ri = 0.01$, (b) $Ri = 0.1$, (c) $Ri = 1.0$ and (d) $Ri = 100$.

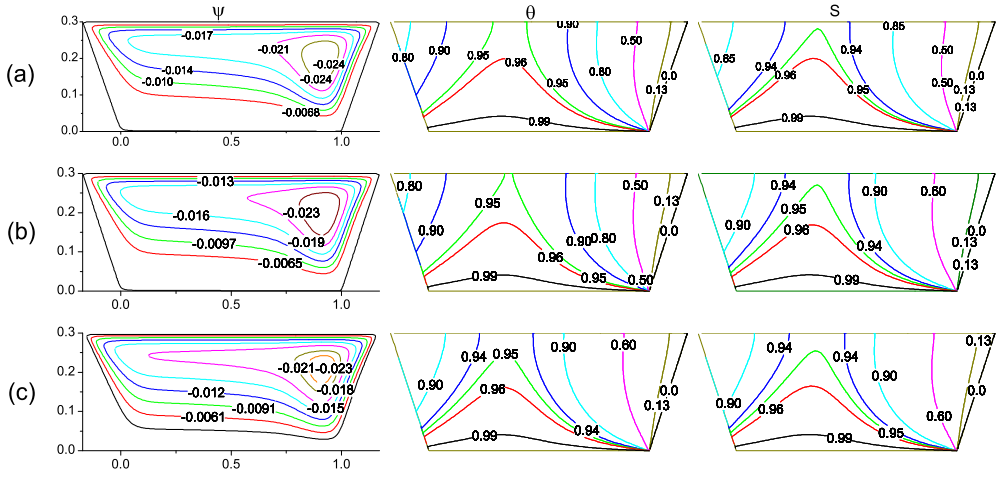

Fig. 4. Streamlines (ψ), isotherms (θ) and isoconcentrations (S) for $Ri = 1$, $Ha = 40$, $N = 1$, $Le = 2$, $Re = 100$ and $A = 0.3$ for (a) $\varphi = 0.01$, (b) $\varphi = 0.05$ and (c) $\varphi = 0.1$.

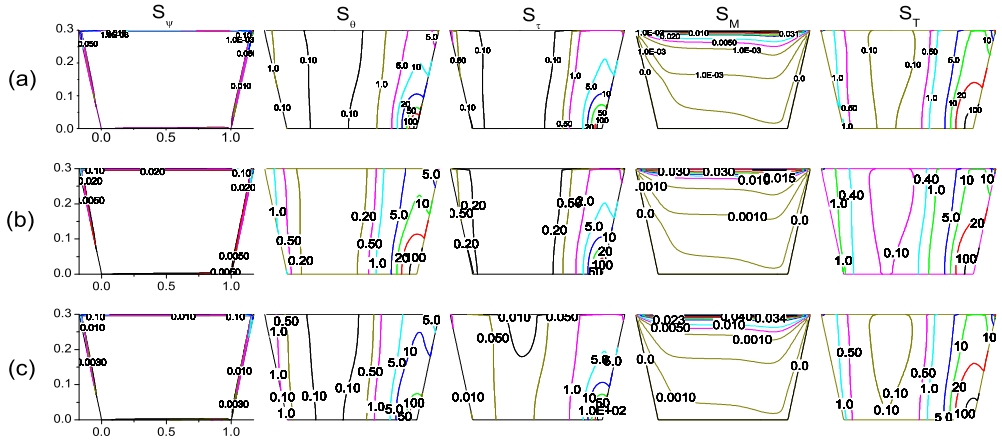

Fig. 5. Entropy generations due to fluid friction (S_ψ), heat transfer (S_θ), mass transfer (S_τ), magnetic field (S_M) and pointwise total entropy generation (S_T) for $N = 5$, $Le = 1$, $Ri = 1$, $Re = 100$, $Ha = 20$ and $A = 0.3$ for (a) $\varphi = 0.01$, (b) $\varphi = 0.05$ and (c) $\varphi = 0.1$.

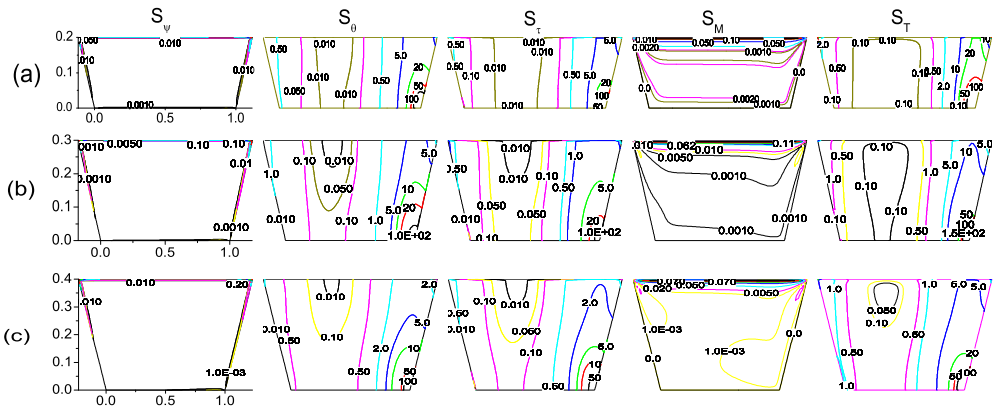

Fig. 6. Entropy generations due to fluid friction (S_ψ), heat transfer (S_θ), mass transfer (S_τ), magnetic field (S_M) and pointwise total entropy generation (S_T) for $N = 5$, $Le = 1$, $Ri = 1$, $Re = 100$, $Ha = 40$, $\phi = 60^0$ and $\varphi = 0.01$ for (a) $A = 0.2$, (b) $A = 0.3$ and (c) $A = 0.4$.

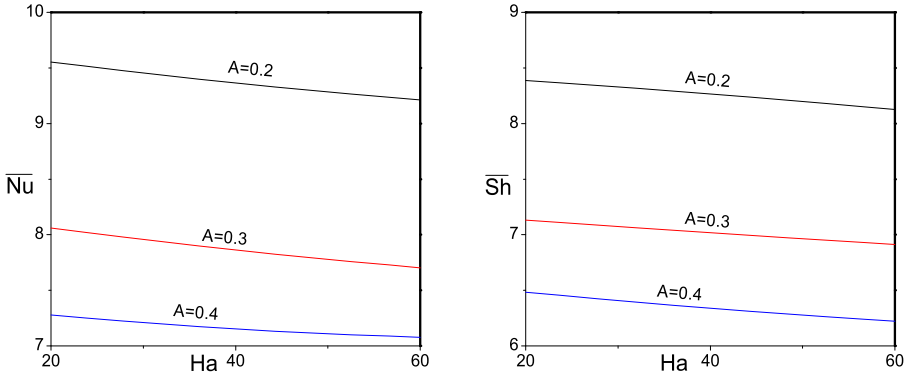

Fig. 7. Variation of average Nusselt number ($\overline{Nu}$) and Sherwood number ($\overline{Sh}$) with Hartmann number (Ha) for $N = 5$, $Le = 1$, $Ri = 1$, $Re = 100$, $\phi = 60^0$, $\varphi = 0.01$ and for various $A(0.2 - 0.4)$.

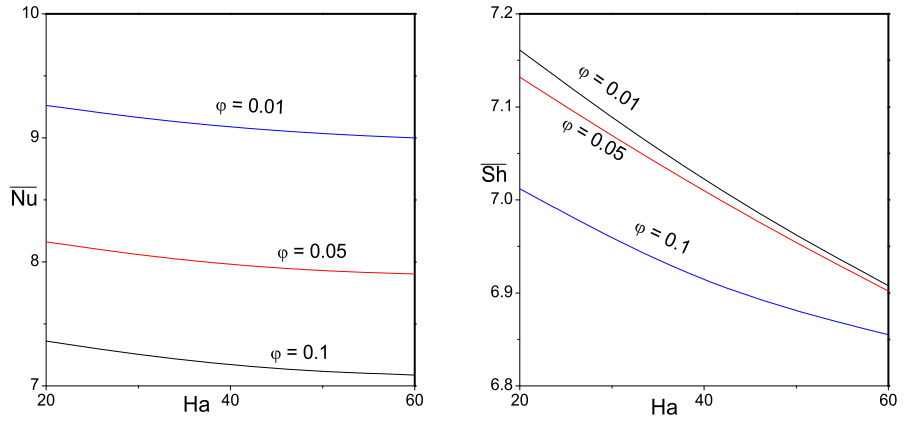

Fig. 8. Variation of average Nusselt number ($\overline{Nu}$) and Sherwood number ($\overline{Sh}$) with Hartmann number (Ha) for $A = 0.3$, $N = 5$, $Le = 1$, $Ri = 1$, $Re = 100$, $\phi = 60^0$, and for various $\varphi(0.01 - 0.1)$.

the increment of φ and the contours of S_M are dense towards the top wall of the cavity caused by the effect of magnetic field acting perpendicularly to the bottom wall of the cavity. The active zones of entropy generations are observed towards the boundary for fluid flow and result a thickness of boundary layer for entropy generation contours due to the no slip boundary conditions. The active zones of entropy generations are found in the right bottom corner for heat and mass transfer where $|S_\theta|_{max}$ and $|S_\tau|_{max}$ occur and near the upper wall for magnetic field where the contours of S_M are dense. This phenomenon is observed for the contours of S_M because the magnetic field is acting in the upward direction.

Figs. 6(a) - 6(c) represents the entropy generation contours for $Ri = 1$, $Ha = 40$, $N = 5$, $Le = 1$, $Re = 100$, $\phi = 60^0$, $\varphi = 0.01$ and for various values of A (0.2, 0.3 and 0.4) with $|S_\psi|_{max}$ = 71.2114 (for $A = 0.2$), 31.645 (for $A = 0.3$), 17.803 (for $A = 0.4$), $|S_\theta|_{max}$ = 714540 (for $A = 0.2$), 317573 (for $A = 0.3$), 178635 (for $A = 0.4$), $|S_\tau|_{max}$ = 354166 (for $A = 0.2$), 157407 (for $A = 0.3$), 88541 (for $A = 0.4$), $|S_M|_{max}$ = 0.1332 (for $A = 0.2$), 0.1233 (for $A = 0.3$), 0.1140 (for $A = 0.4$). The contours of total entropy generation are distributed from bottom wall to top and right walls of the cavity and maximum values are observed in the right bottom corner. These numerical data and contours of Fig. 6 show that the entropy generation is highly dependent on heat

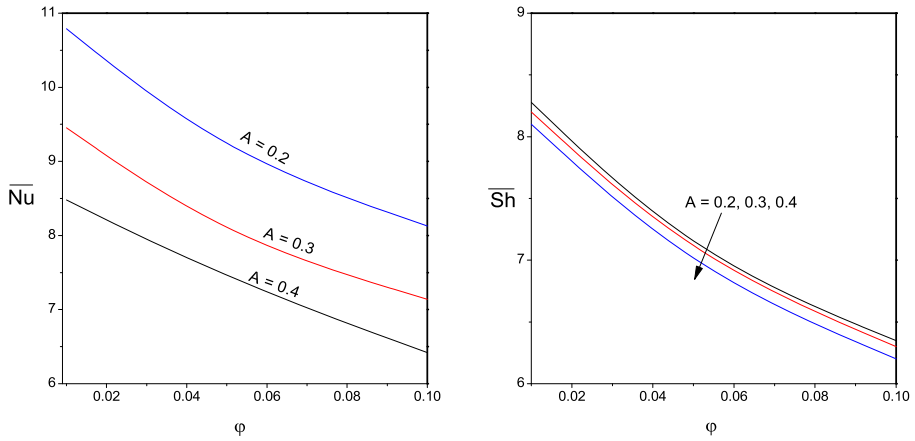

Fig. 9. Variation of average Nusselt number ($\overline{\mathrm{Nu}}$) and Sherwood number ($\overline{Sh}$) with nanoparticle volume fraction φ for $N = 5$, $Le = 1$, $Ri = 1$, $Re = 100$, $Ha = 40$, $\phi = 60^0$, and for various $A(0.2 - 0.4)$.

and mass transfer. So it is clear that increment of aspect ratio will minimize entropy generation of the cavity. On the other hand, electronic equipments and engines should be smaller in size to handle them easily. For this purpose aspect ratio must be kept low and the total entropy generation should be minimum to get the maximum efficiency of a system.

The rate of heat and mass transfer at the wall of the cavity in terms of average Nusselt and Sherwood number have been plotted in Figs. 7, 8, 9. Fig. 7 shows the variation of $\overline{\mathrm{Nu}}$ and $\overline{Sh}$ with respect to Ha for various A when other parameters are fixed. It is observed that $\overline{\mathrm{Nu}}$ and $\overline{Sh}$ are decreasing as Ha and A are decreasing. In Fig. 8 it can be observed that $\overline{\mathrm{Nu}}$ and $\overline{Sh}$ decrease with the increased values of Ha and φ, but in Fig. 9 it is seen that $\overline{\mathrm{Nu}}$ and $\overline{Sh}$ rapidly decrease with the increment of φ and A.

5. Conclusions

As increment of entropy enhances the irreversibilities of a system, one should encounter such kind of system where entropy will be minimum to get the maximum efficiency of any system. Keeping this motivation in mind minimization of entropy generation of a two-dimensional, steady, double-diffusive, mixed convection flow of water - Al_2O_3 nanofluid in a low aspect ratio cavity in the presence of magnetic field has been formulated and solved numerically for a range of Richardson number, aspect ratio, Hartmann number and nanoparticle volume fraction to find out the following conclusions.

As the aspect ratio increases the rate of flow, heat transfer, mass transfer and entropy generations due to fluid flow, heat transfer, mass transfer, and magnetic field increase. This phenomenon is observed due to the increase of fluid volume inside the cavity. So low aspect ratio cavity can be used to minimize entropy generation in various engineering tools and it will save the loss of energy.

The movement of the upper lid of the cavity affects the motion of fluid flow, heat and mass transfer. As Ri increases from 0.01 to 1, i.e., when forced convection phenomenon is changed into mixed convection phenomenon, flow, heat and mass transfer increase. This is caused due to both the effect of natural and forced convection. When $Ri = 100$, i.e., in case of natural convection two-sided circulations from the bottom wall towards left and right walls are observed and fluid flow, heat and mass transfer rates are dominated due to the absence of forced convection. Therefore, entropy generation due to mixed convection (for $Ri = 1$) becomes minimum. So it is concluded that mixed convection phenomenon is more effective than that of natural and forced convection to minimize entropy generation.

As Ha increases, both the rate of heat and mass transfer in terms of Nusselt number and Sherwood number decrease slightly with the increment of aspect ratio. This phenomenon is also observed with the increment of φ. It is also observed that entropy generation increases with the increment of φ. So to minimize entropy generation in a low aspect ratio cavity, nanoparticle volume fraction should be less than 10 per cent and if there is a magnetic field acting perpendicularly to the bottom wall for which the entropy generation is higher towards the upper wall than the low aspect ratio cavity will be useful to minimize entropy generation.

Therefore, the present study concluded that to get significant efficiency of a system and to minimize entropy generation in a low aspect ratio cavity mixed convection flow with a low percentage of nanoparticle volume fraction can be used in a trapezoidal cavity of inclination angle 60^0 when other parameters Le, N, Re, Pr etc. are fixed.

Declarations

Author contribution statement

Priyajit Mondal: Conceived and designed the experiments; Performed the experiments; Wrote the paper.

T.R. Mahapatra: Analyzed and interpreted the data; Wrote the paper.

Rujda Parveen: Conceived and designed the experiments; Wrote the paper.

Funding statement

T.R. Mahapatra was supported by SAP (DRS Phase-III, Letter No. F.510/3/DRS-III/2015(SAPI)) under UGC, New Delhi, India. Rujda Parveen was supported by the Department of Science and Technology (DST) INSPIRE (No: DST/INSPIRE Fellowship/[IF170617]), India.

Data availability statement

Data included in article/supp. material/referenced in article.

Declaration of interests statement

The authors declare no conflict of interest.

Additional information

No additional information is available for this paper.

Acknowledgements

The authors thank the referees for their valuable comments, which enable to produce an improved presentation of their paper.

References

[1] A. Bejan, Entropy Generation Through Heat and Fluid Flow, Wiley and Sons, 1994.
[2] T. Basak, R.S. Kaluri, A.R. Balakrishnanand, Entropy generation during natural convection in a porous cavity: effect of thermal boundary conditions, Numer. Heat Transf. 62 (2012) 336–364.
[3] S.U.S. Choi, Enhancing thermal conductivity of fluids with nanoparticles, developments and applications of non-Newtonian flows, in: D.A. Siginer, H.P. Wang (Eds.), FED—vol. 231/MD—vol. 66, The American Society of Mechanical Engineers, New York, vol. 21, 1995, pp. 99–105.
[4] J. Buongiorno, Convective transport in nanofluids, ASME J. Heat Transf. 128 (3) (2006) 240–250.
[5] S.K. Das, S.U.S. Choi, W. Yu, T. Pradet, Nanofluids: Science and Technology, Wiley, New York, 2007.
[6] D. Wen, G. Lin, S. Vafaei, K. Zhang, Review of nanofluids for heat transfer applications, Particuology 7 (2) (2007) 141–150.
[7] O. Mahian, A. Kianifar, S.A. Kalogirou, I. Pop, S. Wongwises, A review of the applications of nanofluids in solar energy, Int. J. Heat Mass Transf. 52 (2) (2013) 582–594.
[8] R.K. Nayak, S. Bhattacharyya, I. Pop, Effects of nanoparticles dispersion on the mixed convection of a nanofluid in a skewed enclosure, Int. J. Heat Mass Transf. 125 (2018) 908–919.
[9] E. Firouzfar, M. Soltanieh, S.H. Noie, M.H. Saidi, Application of heat pipe heat exchangers in heating, ventilation and air conditioning (HVAC) systems, Sci. Res. Essays 6 (9) (2011) 1900–1908.
[10] K. Hooman, H. Gurgenci, Porous medium modeling of air - cooled condensers, Transp. Porous Media 84 (2010) 257–273.
[11] N. Targui, H. Kahalerras, Analysis of fluid flow and heat transfer in a double pipe heat exchanger with porous structures, Energy Convers. Manag. 49 (2008) 3217–3229.
[12] L.A.B. Pilkington, Review lecture: the float glass process, Proc. R. Soc. Lond. A 314 (1969) 1–25.
[13] F.J.K. Ideriah, Prediction of turbulent cavity flow driven by buoyancy and shear, J. Mech. Eng. Sci. 22 (1980) 287–295.
[14] C.K. Cha, Y. Jaluria, Recirculating mixed convection flow for energy extraction, Int. J. Heat Mass Transf. 27 (1984) 1801–1810.
[15] X. Fang, H.G. Stefan, Dynamics of heat exchange between sediment and water in a lake, Water Resour. Res. 32 (6) (1996) 1719–1727.
[16] H. Khorasanizadeh, M. Nikfar, J. Amani, Entropy generation of Cu–water nanofluid mixed convection in a cavity, Eur. J. Mech. B, Fluids 37 (2013) 143–152.
[17] R.K. Nayak, S. Bhattacharyya, I. Pop, Numerical study on mixed convection and entropy generation of Cu–water nanofluid in a differentially heated skewed enclosure, Int. J. Heat Mass Transf. 85 (2015) 620–634.
[18] H.M. Elshehabey, S.E. Ahmed, MHD mixed convection in a lid-driven cavity filled by a nanofluid with sinusoidal temperature distribution on the both vertical walls using Buongiorno's nanofluid model, Int. J. Heat Mass Transf. 88 (2015) 181–202.
[19] E. Abu-Nada, A.J. Chamkha, Mixed convection flow in a lid-driven inclined square enclosure filled with a nanofluid, Eur. J. Mech. B, Fluids 29 (2010) 472–482.
[20] M.A. Waheed, Mixed convective heat transfer in rectangular enclosures driven by a continuously moving horizontal plate, Int. J. Heat Mass Transf. 52 (2009) 5055–5063.
[21] A.K. Hussein, H.K. Hamzah, F.H. Ali, L. Kolsi, Mixed convection in a trapezoidal enclosure filled with two layers of nanofluid and porous media with a rotating circular cylinder and a sinusoidal bottom wall, J. Therm. Anal. Calorim. 141 (2020) 2061–2079.
[22] R. Parveen, T.R. Mahapatra, Numerical simulation of MHD double diffusive natural convection and entropy generation in a wavy enclosure filled with nanofluid with discrete heating, Heliyon 5 (2019) e02496.
[23] A.J. Chamkha, F. Selimefendigil, H.F. Öztop, Effects of a rotating cone on the mixed convection in a double lid-driven 3D porous trapezoidal nanofluid filled cavity under the impact of magnetic field, Nanomaterials 10 (3) (2020) 449.
[24] D.S. Cimpean, M.A. Sheremet, I. Pop, Mixed convection of hybrid nanofluid in a porous trapezoidal chamber, Int. Commun. Heat Mass Transf. 116 (2020) 104627.
[25] Y. Xuan, W. Roetzel, Conceptions for heat transfer correlation of nanofluids, Int. J. Heat Mass Transf. 43 (19) (2000) 3701–3707.
[26] E. Abu-Nada, Z. Masoud, A. Hijazi, Natural convection heat transfer enhancement in horizontal concentric annuli using nanofluids, Int. Commun. Heat Mass Transf. 35 (5) (2008) 657–665.
[27] J.C. Maxwell-Garnett, Colours in metal glasses and in metallic films, Philos. Trans. R. Soc. Ser. A 203 (1904) 385–420.
[28] H.C. Brinkman, The viscosity of concentrated suspensions and solution, J. Chem. Phys. 20 (1952) 571–581.
[29] J.A. Shercliff, A Text Book of Magnetohydrodynamics, Pergamon Press, 1965.
[30] A. Bejan, Entropy Generation Minimization, CRC Press, Boca Raton, FL, 1996.
[31] A. Bejan, A study of entropy generation in fundamental convective heat transfer, ASME J. Heat Transf. 101 (4) (1979) 718–725.
[32] T.R. Mahapatra, P. Mondal, Heatline and massline analysis due to magnetohydrodynamic double diffusive natural convection in a trapezoidal enclosure with various aspect ratios, Int. J. Appl. Comput. Math. 5 (2019) 82.
[33] T.R. Mahapatra, B.C. Saha, D. Pal, Magnetohydrodynamic double - diffusive natural convection for nanofluid within a trapezoidal enclosure, Comput. Appl. Math. 37 (2018) 6132–6151.
[34] M.M. Gupta, J.C. Kalita, A new paradigm for solving Navier-Stokes equations: streamfunction - velocity formulation, J. Comput. Phys. 207 (2005) 52–68.
[35] B. Ghasemi, S.M. Aminossadati, A. Raisi, Magnetic field effect on natural convection in a nanofluid-filled square enclosure, Int. J. Therm. Sci. 50 (2011) 1748–1756.